The EUMETSAT
Network of
Satellite Application
Facilities

H SAF

Support to Operational
Hydrology and Water
Management

Italian Meteorological Service

Italian Department of Civil Defence

Algorithm Theoretical Definition Document (ATDD)
for product

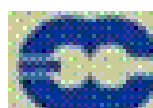# SN-OBS-3 - Effective snow cover by VIS/IR radiometry

ZAMG
Zentralanstalt für Meteorologie und Geodynamik

Vienna University of Technology Institut für Photogrammetrie und Fernerkundung

RMI
Royal Meteorological Institute of Belgium

European Centre for Medium-Range Weather Forecasts

Finnish Meteorological Institute

SYKE
Finnish Environment Institute

TKK
Helsinki University of Technology

Météo-France

LATMOS
CNRS Laboratoire Atmosphères, Milieux, Observations Spatiales

CESBIO
CNRS Centre d'Etudes Spatiales de la BIOsphere

bfg Bundesanstalt für Gewässerkunde
Bundesanstalt für Gewässerkunde

OMSZ
Hungarian Meteorological Service

ISAC
CNR - Istituto Scienze dell'Atmosfera e del Clima

Università di Ferrara

Institute of Meteorology and Water Management

NMA
Romania National Meteorological Administration

SHMU
Slovak Hydro-Meteorological Institute

METEOROLOJI
Turkish State Meteorological Service

Middle East Technical University

Istanbul Technical University

Anadolu University

30 May 2010

Algorithm Theoretical Definition Document ATDD-12
Product SN-OBS-3
Effective snow cover by VIS/IR radiometry

INDEX

List of Tables

List of Figures

Acronyms

AAPP	ATOVS and AVHRR Processing Package
ATDD	Algorithms Theoretical Definition Document
AU	Anadolu University (in Turkey)
AVHRR	Advanced Very High Resolution Radiometer (on NOAA and MetOp)
AWOS	Automated Weather Observing Stations
BfG	Bundesanstalt für Gewässerkunde (in Germany)
BRDF	Bi-directional Reflectance Distribution Function
CAF	Central Application Facility (of EUMETSAT)
CDA	Command and Data Acquisition station
CESBIO	Centre d'Etudes Spatiales de la BIOsphere (of CNRS, in France)
CM-SAF	SAF on Climate Monitoring
CNMCA	Centro Nazionale di Meteorologia e Climatologia Aeronautica (in Italy)
CNR	Consiglio Nazionale delle Ricerche (of Italy)
CNRS	Centre Nationale de la Recherche Scientifique (of France)
DEM	Digital Elevation Model
DPC	Dipartimento Protezione Civile (of Italy)
DWD	Deutscher Wetterdienst
EARS	EUMETSAT Advanced Retransmission Service
ECMWF	European Centre for Medium-range Weather Forecasts
EOS	Earth Observing System (*Terra*, *Aqua*, *Aura*)
EUM	Short for EUMETSAT
EUMETCast	EUMETSAT's Broadcast System for Environmental Data
EUMETSAT	European Organisation for the Exploitation of Meteorological Satellites
FMI	Finnish Meteorological Institute
FPAR	Fraction of Photosynthetically Active Radiation
GEO	Geostationary Earth Orbit
GRAS-SAF	SAF on GRAS Meteorology
GTOPO	Global digital elevation model (U.S. Geological Survey)
HRPT	High Resolution Picture Transmission
H-SAF	SAF on Support to Operational Hydrology and Water Management
IFOV	Instantaneous Field Of View
IMWM	Institute of Meteorology and Water Management (in Poland)
IPF	Institut für Photogrammetrie und Fernerkundung (of TU-Wien, in Austria)
IR	Infra Red
IRM	Institut Royal Météorologique (of Belgium) (alternative of RMI)
ISAC	Istituto di Scienze dell'Atmosfera e del Clima (of CNR, Italy)
ITU	İstanbul Technical University (in Turkey)
LAI	Leaf Area Index
LATMOS	Laboratoire Atmosphères, Milieux, Observations Spatiales (of CNRS, in France)
LEO	Low Earth Orbit
LSA-SAF	SAF on Land Surface Analysis
Météo France	National Meteorological Service of France
MetOp	Meteorological Operational satellite
METU	Middle East Technical University (in Turkey)
MODIS	Moderate-resolution Imaging Spectro-radiometer (on EOS Terra and Aqua)
MW	Micro Wave
NASA	National Aeronautical and Space Administration (in USA)
NCEP	National Centers for Environmental Prediction (in NOAA)
NDSI	Normalized Difference Snow Index
NMA	National Meteorological Administration (of Romania)
NOAA	National Oceanic and Atmospheric Administration (Agency and satellite)

NWC	Nowcasting
NWC-SAF	SAF in support to Nowcasting & Very Short Range Forecasting
NWP	Numerical Weather Prediction
NWP-SAF	SAF on Numerical Weather Prediction
O3M-SAF	SAF on Ozone and Atmospheric Chemistry Monitoring
OMSZ	Hungarian Meteorological Service
OSI-SAF	SAF on Ocean and Sea Ice
Pixel	Picture element
PUM	Product User Manual
PVR	Product Validation Report
REP-3	H-SAF Products Validation Report
RMI	Royal Meteorological Institute (of Belgium) (alternative of IRM)
SAF	Satellite Application Facility
SCA	Snow Covered Area
SD	Snow Depth
SHMÚ	Slovak Hydro-Meteorological Institute
STD	Standard Deviation
STRM	Shuttle Radar Topographic Mission
SVRR	System Validation Results Review
SWE	Snow Water Equivalent
SYKE	Suomen ympäristökeskus (Finnish Environment Institute)
TKK	Teknillinen korkeakoulu (Helsinki University of Technology)
TSMS	Turkish State Meteorological Service
TU-Wien	Technische Universität Wien (in Austria)
UniFe	University of Ferrara (in Italy)
VIS	Visible
ZAMG	Zentralanstalt für Meteorologie und Geodynamik (of Austria)

1.   The EUMETSAT Satellite Application Facilities and H-SAF

The "*EUMETSAT Satellite Application Facility on Support to Operational Hydrology and Water Management (H-SAF)*" is part of the distributed application ground segment of the "*European Organisation for the Exploitation of Meteorological Satellites (EUMETSAT)*". The application ground segment consists of a "*Central Application Facility (CAF)*" and a network of eight "*Satellite Application Facilities (SAFs)*" dedicated to development and operational activities to provide satellite-derived data to support specific user communities. See ***Fig. 01***.
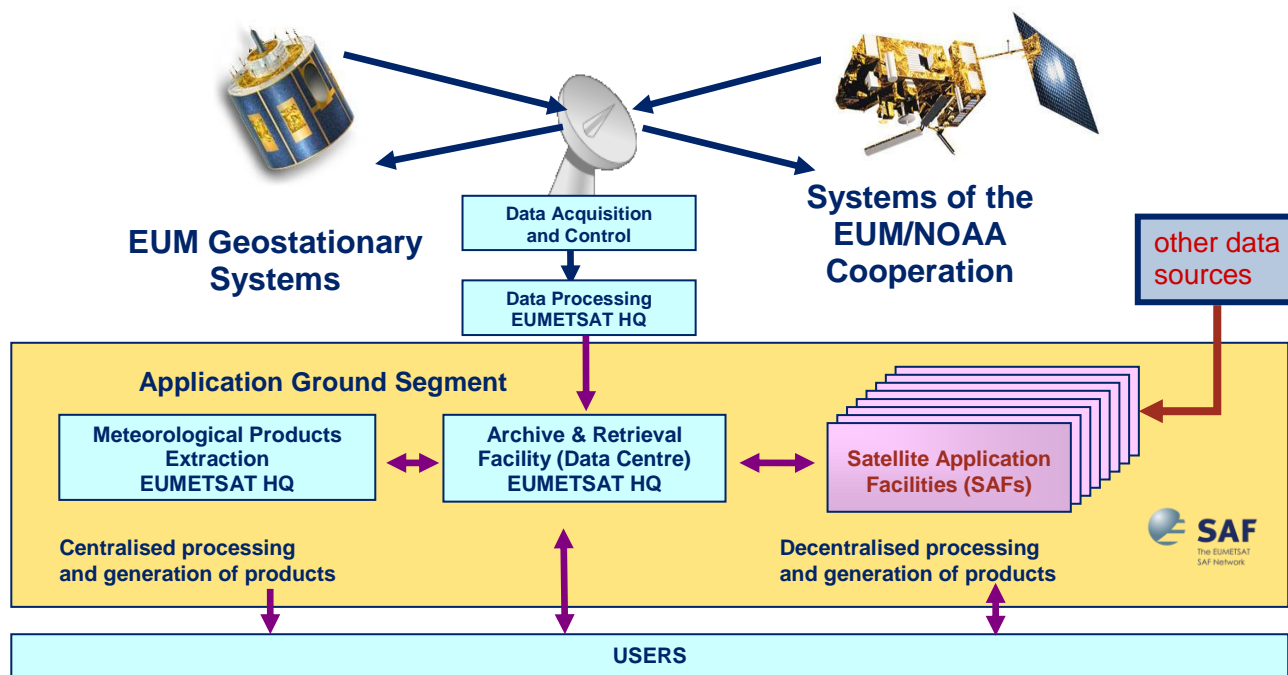
Fig. 01 - Conceptual scheme of the EUMETSAT application ground segment.

Fig. 02 reminds the current composition of the EUMETSAT SAF network (in order of establishment).

Fig. 02 - Current composition of the EUMETSAT SAF network (in order of establishment).

The H-SAF was established by the EUMETSAT Council on 3 July 2005; its Development Phase started on 1st September 2005 and ends on 31 August 2010. The list of H-SAF products is shown in ***Table 01***.

Table 01 - List of H-SAF products

Code	Acronym	Product name
H01	PR-OBS-1	Precipitation rate at ground by MW conical scanners (with indication of phase)
H02	PR-OBS-2	Precipitation rate at ground by MW cross-track scanners (with indication of phase)
H03	PR-OBS-3	Precipitation rate at ground by GEO/IR supported by LEO/MW
H04	PR-OBS-4	Precipitation rate at ground by LEO/MW supported by GEO/IR (with flag for phase)
H05	PR-OBS-5	Accumulated precipitation at ground by blended MW and IR
H06	PR-ASS-1	Instantaneous and accumulated precipitation at ground computed by a NWP model
H07	SM-OBS-1	Large-scale surface soil moisture by radar scatterometer
H08	SM-OBS-2	Small-scale surface soil moisture by radar scatterometer
H09	SM-ASS-1	Volumetric soil moisture (roots region) by scatterometer assimilation in NWP model
H10	SN-OBS-1	Snow detection (snow mask) by VIS/IR radiometry
H11	SN-OBS-2	Snow status (dry/wet) by MW radiometry
H12	SN-OBS-3	Effective snow cover by VIS/IR radiometry
H13	SN-OBS-4	Snow water equivalent by MW radiometry

2. Introduction to product SN-OBS-3

2.1 Sensing principle

Product SN-OBS-3 (*Effective snow cover by VIS/IR radiometry*) is based on multi-channel analysis of the AVHRR instrument onboard NOAA and MetOp satellites. The AVHRR radiometer has an IFOV of 1.1 x 1.1 km^2 at nadir degrading to ~ 2 x 6 km^2 at the edge of the 2900 km cross-track swath. Computing fractional cover would in principle require segmenting the image in arrays of pixels (typically ~ 32 x 32) and counting those classifies as snow. This would lead to unacceptable product resolution. For H-SAF, fractional cover is generated at pixel resolution, by exploiting the brightness intensity that is the convolution of the snow signal (highest) and the fraction of snow within the pixel ("effective" cover").
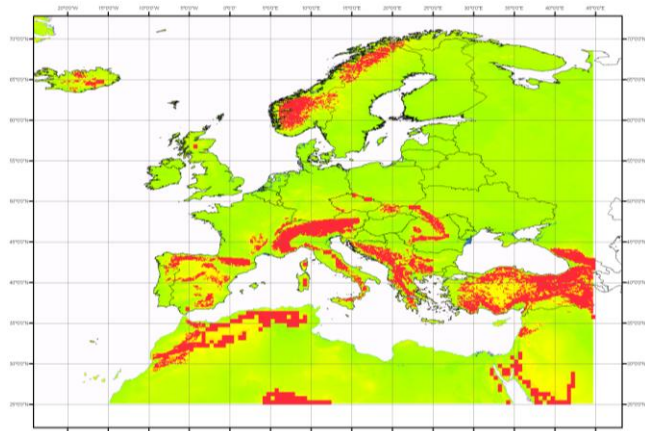
Fig. 03 - Mask flat/forested versus mountainous regions.

The retrieval algorithm is somewhat different for flat or forested area and for mountainous regions. PR-OBS-3 is generated in Finland by FMI and in Turkey by TSMS. The products from FMI and from TSMS both cover the full H-SAF area, but thereafter are merged at FMI by blending the information on flat/forested areas from the FMI product and that one on mountainous areas from the TSMS product, according to the mask shown in ***Fig. 03***.

The observing cycle of the complex of NOAA and MetOp satellites over Europe is about 3 h. For a single satellite pass, several areas in the scene would provide no useful measurements because of clouds. Therefore, the complex of passes is multi-temporally analysed to search for time instants of cloud-free conditions in a given time interval (e.g., 24 h). However, since short-wave channels play an essential role in the retrieval algorithm, the useful range of hours is in daylight.

For more information, please refer to the Products User Manual (specifically, volume PUM-12).

2.2 Main operational characteristics

The operational characteristics of SN-OBS-3 are discussed in PUM-12. Here are the main highlights.

The horizontal resolution (Δx) descends from the AVHRR Instantaneous Field of View (*IFOV*), that is ~ 2 km (average across the swath). Sampling is made at 0.01-degree intervals. Conclusion:

* resolution Δx ~ 2 km - sampling distance: ~ 1 km.

The *observing cycle (Δt)*. In order to collect as many cloud-free pixels as possible, multi-temporal analysis over 24 hours is performed. Thus:

* observing cycle: Δt = 24 h.

The *timeliness (δ)*. For a product resulting from multi-temporal analysis disseminated at a fixed time of the day, the time of observation may change pixel by pixel (some pixel may have been cloud-free early in the time window, e.g. in the early morning, thus up to 12-h old at the time of dissemination; some very recently, just before product dissemination in the late afternoon). Thus the average timeliness is:

* timeliness δ ~ 6 h.

The *accuracy* is evaluated *a-posteriori* by means of the validation activity. See Product Validation Report PVR-12.

2.3 Architecture of the product generation chain

The architecture of the SN-OBS-3 product generation chain is shown in *Fig. 04*
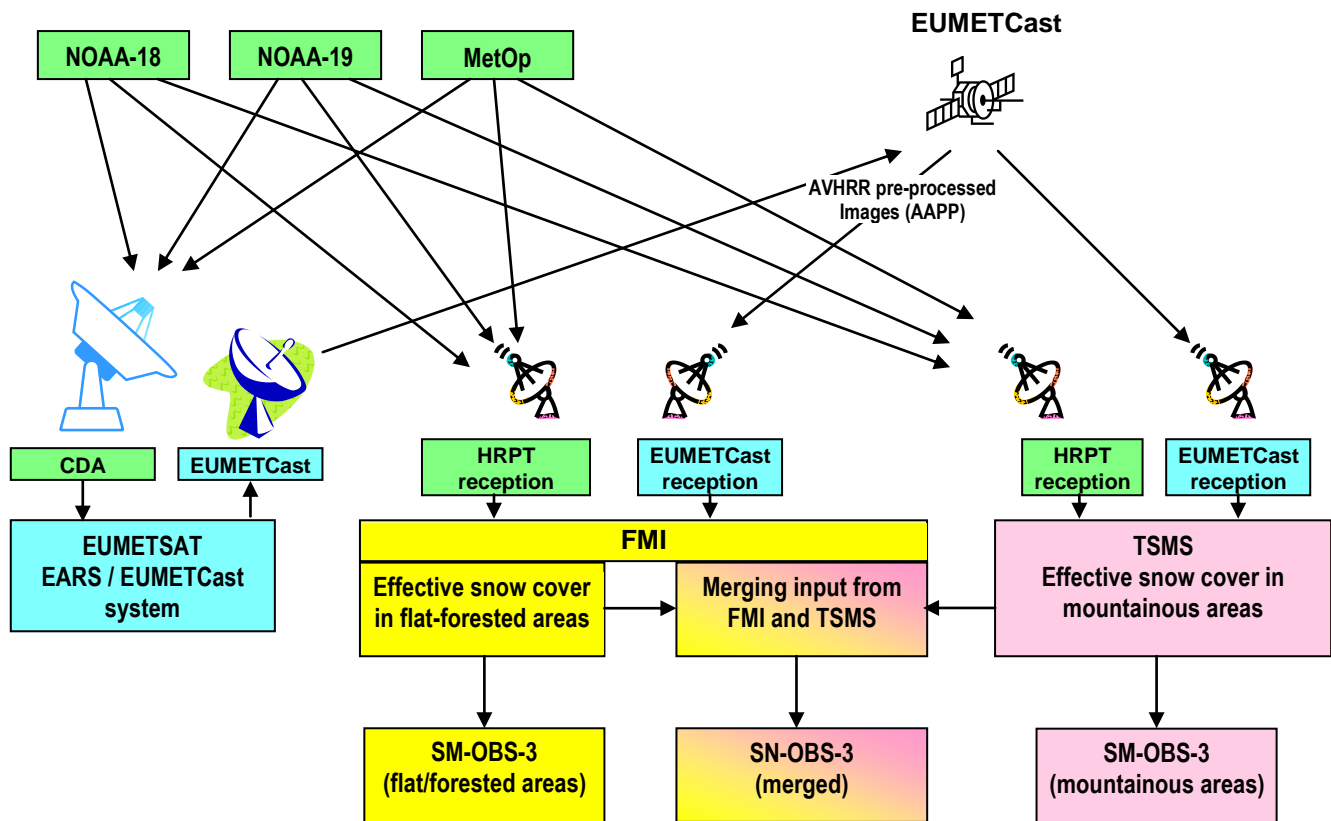
Fig. 04 - Conceptual architecture of the SN-OBS-3 chain.

It is noted that the satellite data are acquired either by direct-read-out through the HRPT system, or via EUMETCast to cover H-SAF areas outside the acquisition range of the HRPT station. The product is generated both at FMI and at TSMS. The FMI product is tuned to flat/forested areas, that one from TSMS is tuned to mountainous areas. The TSMS data are delivered to FMI, that implements the merging of the two products according to the mask shown in Fig. 03.

Currently, the products are held on the TSMS server (mountainous areas) and on the FMI and CNMCA servers (both flat/forested areas and merged). Eventually, only the merged product will be disseminated through EUMETCast.

2.4 Product development team

Names and coordinates of the main actors for SN-OBS-3 algorithm development and integration are listed in *Table 02*.

Table 02 - Development team for product SN-OBS-3

Jouni Pulliainen (Leader)	Finnish Meteorological Institut (FMI)	Finland	jouni.pulliainen@fmi.fi
Panu Lahtinen			panu.lahtinen@fmi.fi
Kati Anttila			kati.anttila@fmi.fi
Sari Metsämäki	Finnish Environment Institute (SYKE)		sari.metsamaki@ymparisto.fi
Ali Ünal Sorman (Co-leader)	Middle East Technical University (METU)	Turkey	sorman@metu.edu.tr
Zuhal Akyurek			zakyurek@metu.edu.tr

3.   Processing concept

The approaches selected for different areas (flat/forested vs. mountainous) show directly the different needs for those areas. For forested areas it is essential to take accurate forest transmissivity into account, as for the mountainous areas, this has little effect (few trees). For mountainous areas the sun zenith and azimuth angles, as well as direction of observation relative to these are more limiting factors. The processing concepts for products SN-OBS-3 applied in Finland (FMI) and Turkey (METU) are somewhat different. They are recorded independently.

3.1   Flat and forested areas   [SYKE]

Fig. 05 illustrates the flow chart of the processing chain for effective snow cover retrieval. The offline activity shows the parts consisting of semi-static databases. Snow cover results are added in the effective snow cover time series database for use in mosaic processing snow cover area (SCA) -maps from different areas, if needed.

The transmissivity map is essential input to the SCA-model, and has to be generated from reflectance data acquired at full dry snow cover conditions for each unit-area of the product. The cloud detections rules are the same as described in ATDD-10 for the Snow recognition model.
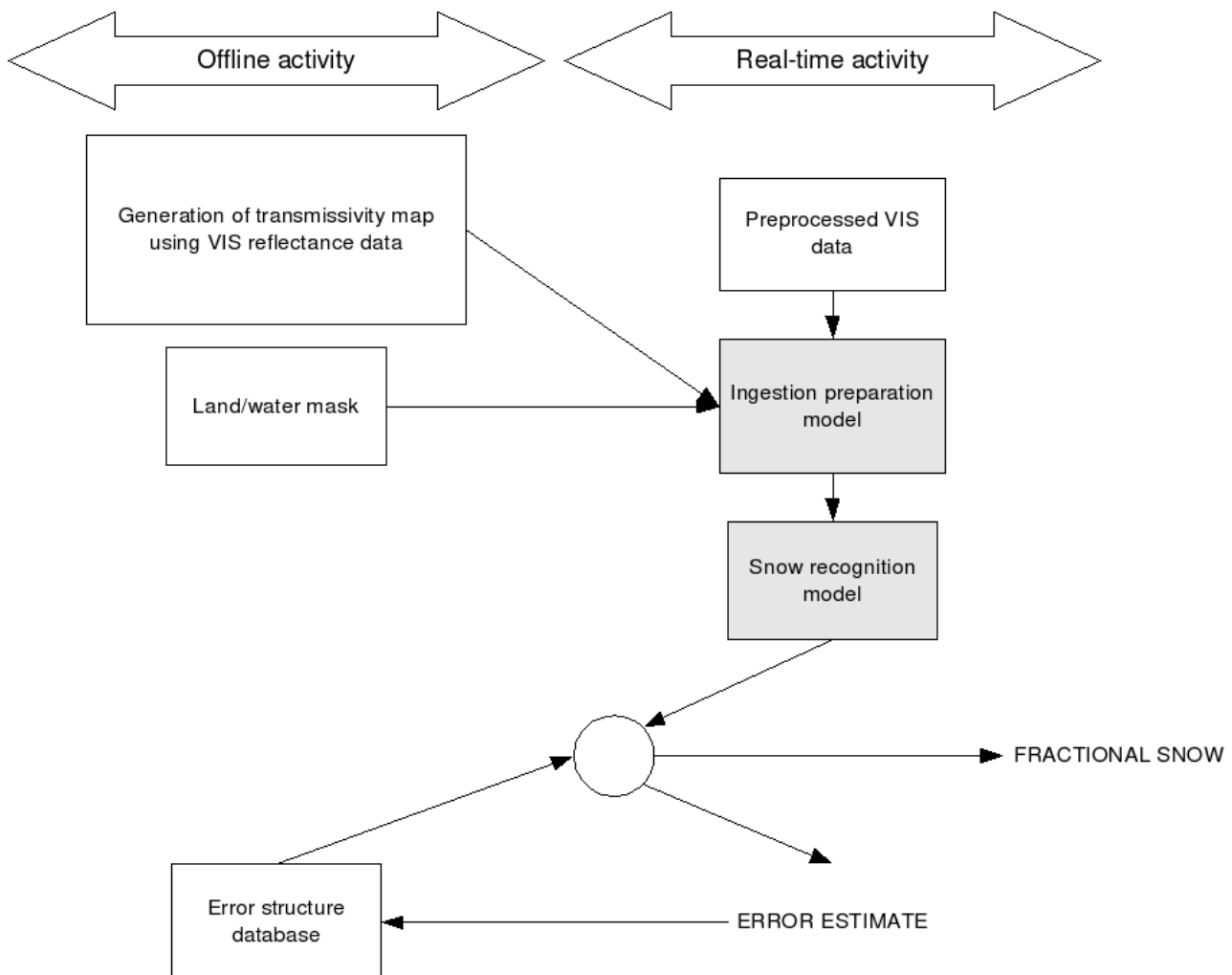
Fig. 05 - Snow covered area generation chain for flat/forested areas.

3.2   Mountainous regions   [METU]

Topography has an effect on satellite-measured radiances. For mountainous terrain three effects that caused by the topography can be listed: 1) Some areas receive exclusively diffuse irradiance due to cast shadows; 2) Shielding of the sky hemisphere reduces the diffuse irradiance; and 3) surrounding terrain reflects irradiance towards the observed ground area (Proy et al. 1989). The shadowed areas become smaller on slopes facing the sun, while they increase on slopes oriented away from the sun.

Several methods have been developed so far with the purpose of removing terrain effects from the measured pixel radiance. Widely used methods are the Lambertian cosine correction, the statistical-emprical correction, the C-correction and the Minnaert correction (Vikhmar et al. 2004; Riano et al. 2003). The general approach of these methods is to normalize the observed radiance from inclined surfaces (L_T) to flat (horizontal) surfaces (L_H) by modelling the local incidence angle to the terrain surface cos (i) for each pixel (*Table 03*). i (γi) is defined as the angle between the surface normal and the solar beam (*Fig. 06*). Using information about the solar position at the acquisition time for the satellite image and the local terrain relief, i can be calculated for a pixel by the formula (Smith et al. 1980):

$$\cos i = \cos sz \cos tz + \sin sz \sin tz \cos (sa\text{-}ta) \tag{1}$$

where sz(θi) is the solar zenith angle, sa (ϕo)is the solar azimuth angle, tz(θp) is the surface normal zenith angle or the terrain slope and ta (ϕa) is the terrain azimuth angle.

Table 03 - Methods for topographic correction of satellite measured radiance

| Method	Equation
Lambertian cosine correction	$L_H = L_T \left(\dfrac{\cos(sz)}{\cos(i)} \right)$
C-correction	$L_H = L_T \left(\dfrac{\cos(sz) + C}{\cos(i) + C} \right)$
Minnaert correction	$L_H = L_T \left(\dfrac{\cos(sz)}{\cos(i)} \right)^k$
Statistic-empirical correction	$L_H = L_T - \cos(i)m - b + \overline{L_T}$
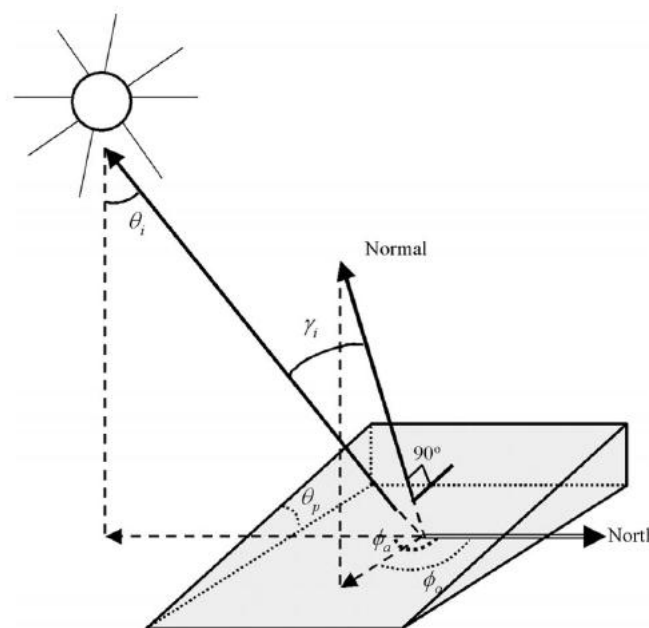
Fig. 06 - Angles involved in the computation of illumination angle (i).

The most critical points for the radiometric correction are bidirectional reflectance effects (atmospheric correction), the spatial resolution of the DEM, and the calculation of slope and aspect from the digital terrain data as topographic factors.

Atmospheric correction

Atmospheric correction is important to obtain the true reflectance of the Earth features. However rather than applying an atmospheric correction method to the downloaded data, atmospherically corrected data are downloaded. In this part MOD02HKM data, which is the calibrated Earth view data at 500 m resolution, and MOD09GKM, which is the land surface reflectances having atmospheric correction, are used. The surface reflectance is inverted with the help of a radiative transfer model (http://modis-sr.ltdri.org/6S_code/index.html) using atmospheric inputs taken from NCEP (ozone, pressure) or directly derived the MODIS data (aerosol, water vapor). The Surface Reflectance product is a major input utilized in the generation of several land products: Vegetation Indices, BRDF, Land Cover, Snow Cover, Thermal Anomalies, and LAI/FPAR.

The NDSI, brief description is given in section 4.2, is calculated for both of the data (***Fig. 07***). It is seen from this figure that NDSI computed from the reflectance values (MOD09) for snow covered pixels have larger scattering compared to the NDSI values computed from the radiances (MOD02). This indicates that for fractional snow cover determination atmospherically corrected satellite data can give better results.
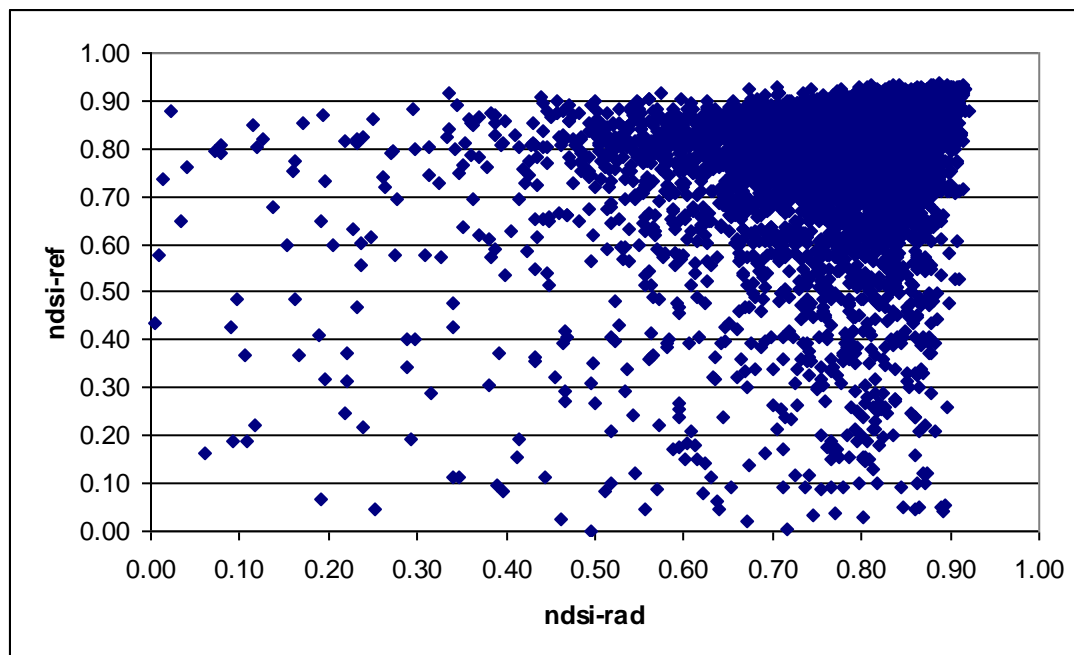
Fig. 07 - NDSI computed from MOD02 radiance (x-axis) and MOD09 reflectance (y-axis) values for March 14, 2006.

Topographic effect

In using the MODIS data Artifacts might arise when the DEM resolution cell is not adequate for the pixel size of the imaging satellite sensor (Richter 1998). DEM having a spatial resolution of 0.25 times the pixel size or better is recommended to be desirable for the topographic correction. Considering the operational products in H-SAF project, SRTM 30 (around 1 km resolution) is the DEM that can be used in the project. At this stage a better DEM having a resolution of 100 m is used to see the effect of the topography for the radiometric correction of MODIS data. The process performed for the topographic correction of the satellite data is summarized in ***Fig. 08***.
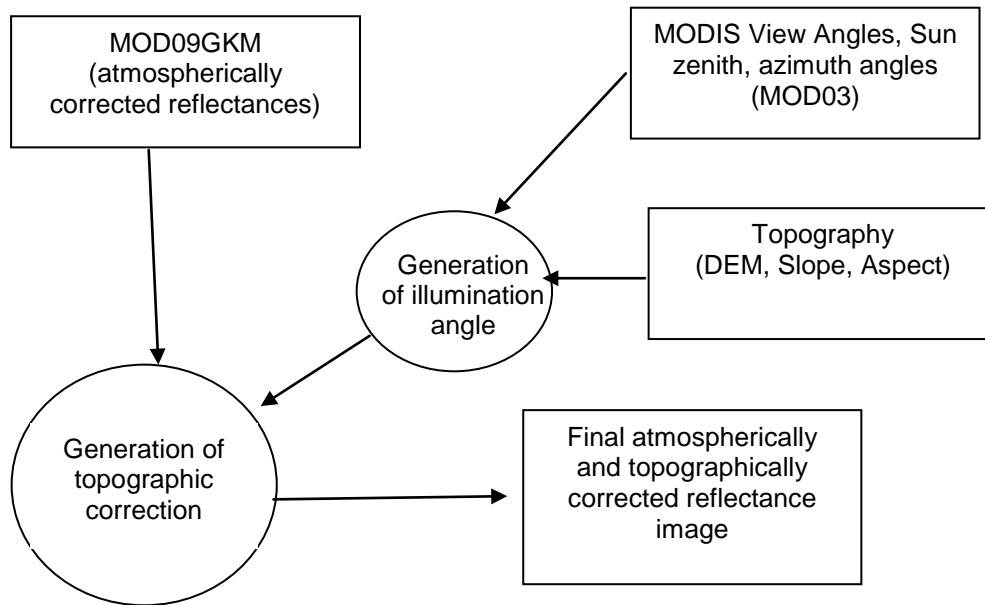
Fig. 08 - The process followed in topographic correction of MODIS data.

As it is summarized in Table 03, all the topographic correction methods are applied for the optic band (Band 4). From the analysis no illumination effect on the infrared band is seen. The effect of these correction methods are given in *Fig. 09*. Considering the correction for two dates (March 14, March 30), the results obtained from the statistic-empirical correction method are comparatively good. In *Fig. 10*, the apparent reflectances and the topographically corrected reflectances are given for March 30, 2006.
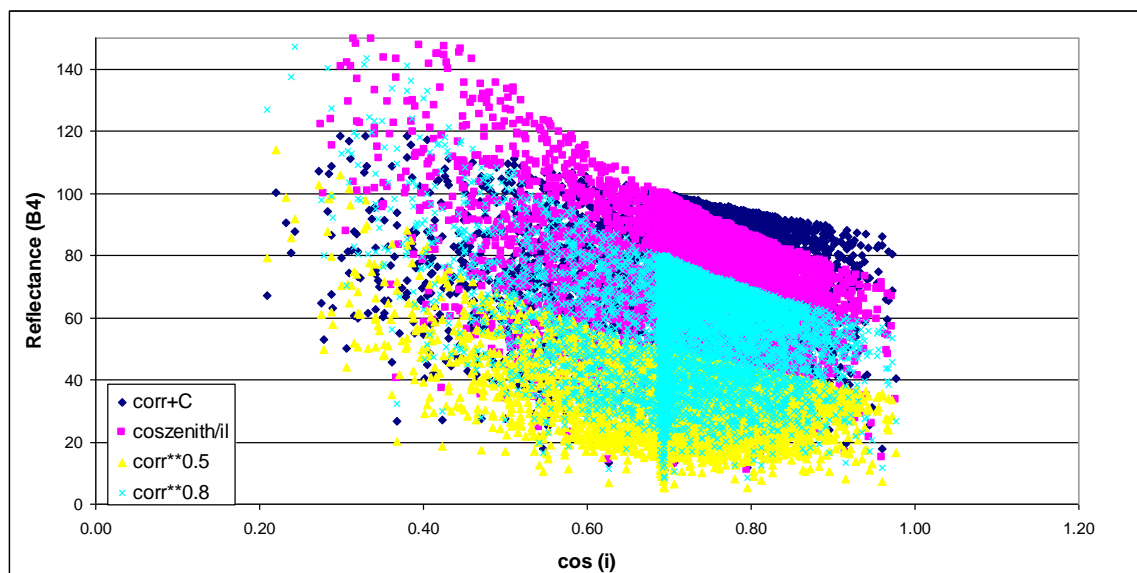
Fig. 09 - The effect of different topographic correction methods on the reflectance for March 16, 2006.

(a)   (b)
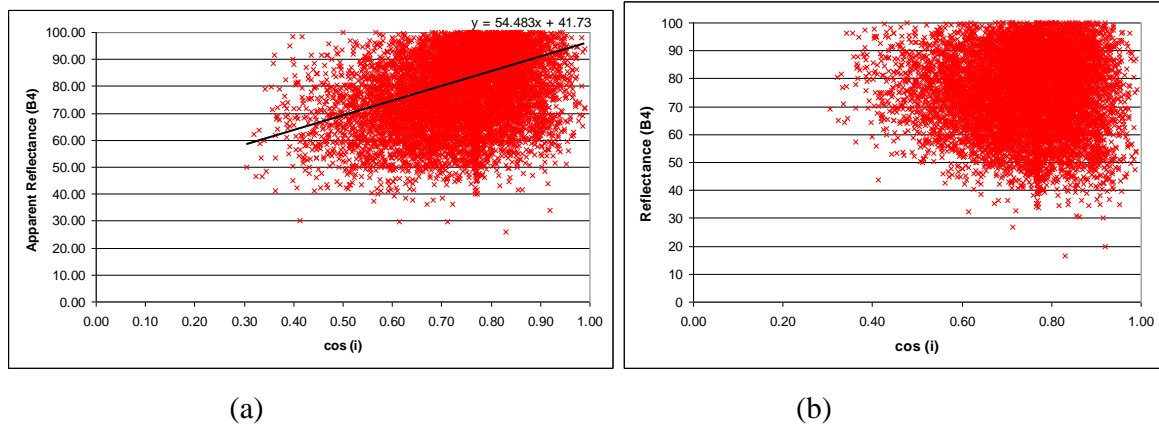
Fig. 10 - The apparent (a) and the topographically corrected (b) reflectances for B4 (0.545-0.565 μm) for March 30, 2006.

Fig. 08 depicts the flowchart of the process for topographic correction and ***Fig. 11*** illustrates the flow chart of the processing chain for effective snow cover retrieval for mountainous areas.
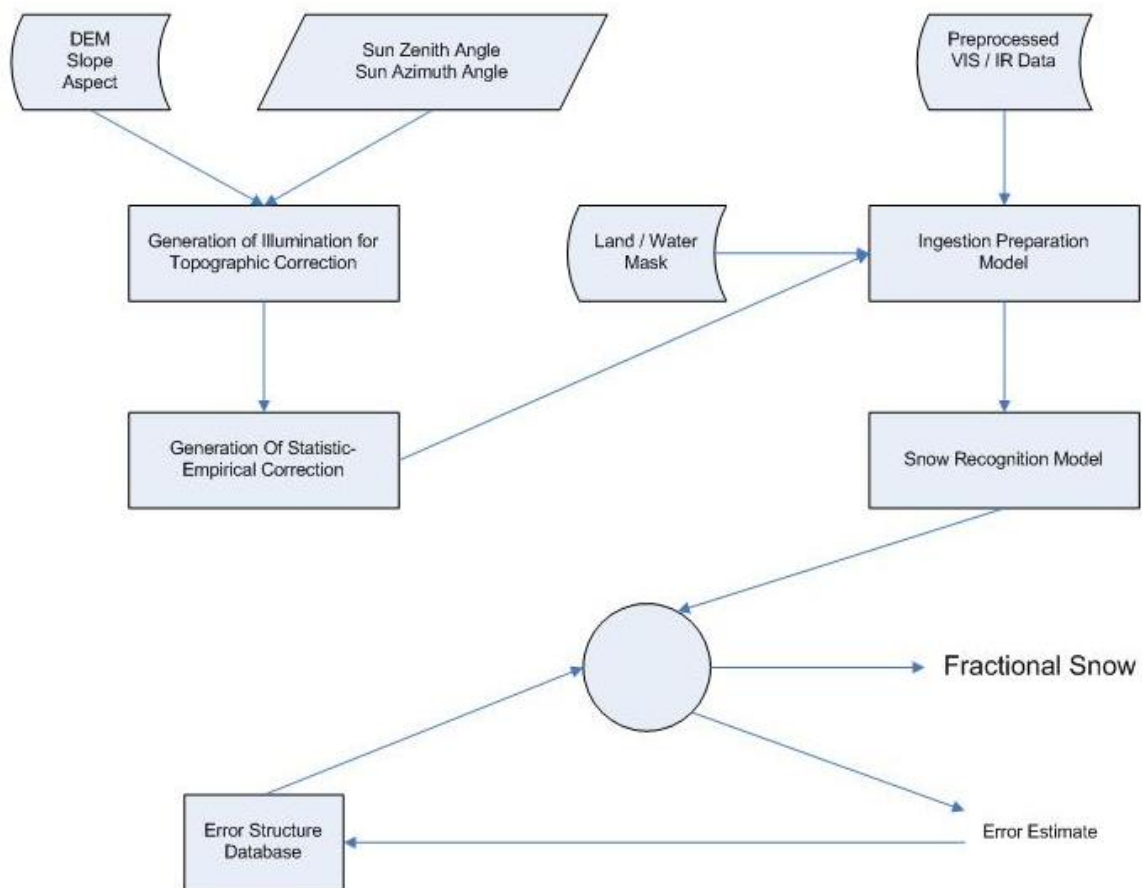
Fig. 11 - Snow covered area generation chain for mountainous areas.

4.   Algorithms description

4.1   Flat and forested areas   [SYKE]

Basis for the fractional snow covered area (SCA) product is algorithm developed by SYKE. The algorithm uses visible and near infrared data. The algorithm is based on a semi-empirical reflectance model, where reflectance from unit area is expressed as a function of SCA. The contributing reflectances from wet snow, forest canopy and snow-free ground serve as model parameters; the key parameter is an average forest transmissivity, which is individually determined for each unit area in Europe using Earth observation data and even using similar data as for the actual SCA-estimation.

The following algorithms have been used with the NOAA/AVHRR and Terra/MODIS data. In later stages, these algorithms will be modified in order to meet the needs for the other instruments.

The method for SCA estimation is based on the high reflectance of snow compared with other natural targets. An empirical model to describe the reflectance as a function of SCA is the basis of the method (Metsämäki et al. 2005):

$$\rho_{\lambda,obs}(SCA) = (1-t^2_{\lambda})\rho_{\lambda,forest} + t^2_{\lambda}[SCA*\rho_{\lambda,snow} + (1-SCA)\rho_{\lambda,ground}], \qquad (1)$$

where $\rho_{\lambda,snow}$, $\rho_{\lambda,ground}$ and $\rho_{\lambda,forest}$ are the generally applicable reflectances for wet snow, snow-free ground and dense coniferous forest canopy at wavelength λ, respectively. $\rho_{\lambda,obs}$ (SCA) stands for the observed reflectance from an areal calculation unit with the current snow cover fraction. t_{λ} stands for effective transmissivity within the calculation unit area. It describes how much of the upwelling radiance is originated from the forest floor and open areas together. Employment of transmissivity allows SCA estimation in all kinds of areas, with forest coverage varying from 0 % to 100 %. Furthermore, a priori information on forests is not needed: the effective transmissivity for each calculation unit area is estimated from satellite-borne reflectance data. This requires reflectance data providing a high contrast between forest canopy and ground not obscured by trees. The required contrast is obtained at visible wavelengths at full dry snow cover conditions (SCA=1). Then, t^2_{λ} is obtained from Eq. (1):

$$t^2_{\lambda} = \frac{\rho_{\lambda,obs}(SCA=1) - \rho_{\lambda,forest}}{\rho_{\lambda,drysnow} - \rho_{\lambda,forest}}, \qquad (2)$$

where $\rho_{\lambda,obs}$ (SCA=1) stands for the observed reflectance at full dry snow cover conditions and $\rho_{\lambda,drysnow}$ stands for the generally applicable dry snow reflectance. Note that employing of dry snow here is advantageous as smaller reflectance variance is gained due to the smaller grain size variation (Warren, 1982); thus leading to better accuracy for transmissivity.

After the effective transmissivity t_{λ} is determined, the SCA is obtained by inverting Eq. (1), as follows:

$$SCA = \frac{\frac{1}{t^2_{\lambda}}*\rho_{\lambda,obs}(SCA) + \left(1-\frac{1}{t^2_{\lambda}}\right)*\rho_{\lambda,forest} - \rho_{\lambda,ground}}{\rho_{\lambda,snow} - \rho_{\lambda,ground}}. \qquad (3)$$

The final SCA represents the average fraction of snow covered ground for the calculation unit area.

In Eq. (1)-(3), the applied wavelength region for reflectance may vary from blue to near-infrared, depending on sensor. With the NOAA/AVHRR, the visible band 1 (580–680 nm) has been used. With MODIS, visible band 4 (545-565 nm) is applied. In these wavelengths, the effect of snow grain size to the reflectance is at its minimum (Warren 1982), which is beneficial for accuracy as one general snow reflectance value is applied throughout the study area. In addition, the chlorophyll absorption peak occurring in this wavelength region enables snow mapping also at the very end of the melting season, as the appearance of seasonal green vegetation disturbs the observed reflectance only slightly. However, visible band reflectance is sensitive to snow impurities (Warren 1982) which increases the reflectance variation and has to be considered in the accuracy assessment.

4.2   Mountainous regions   [METU]

Taking advantage of the fact that snow reflectance is high in the visible (0.5-0.7 μm) wavelengths and has low reflectance in the shortwave infrared (1–4 μm) wavelengths to enable distinguishing snow from clouds and other non-snow-covered conditions, Hall et al. 2002 have used the normalized difference snow index (NDSI) to develop an automated approach to provide daily, global observations of snow cover. The NDSI is defined as the difference of reflectance observed in a visible band such as MODIS band 4 (0.555 μm) and a short-wave infrared band such as MODIS band 6 (1.640 μm) divided by the sum of the two reflectance values.

The fractional snow cover area (SCA) algorithm is based on a sub-pixel reflectance model. Pixel reflectance is modelled as a linear mixture of snow and snow free bare ground. The original model has previously been developed by Vikhamar et al. 2004. In that model pixel reflectance is modelled as a linear mixture of snow, individual tree species and snow-free bare ground (e.g. rock, soil, low vegetation):

$$\overline{R} = A_p R_p + A_s R_s + A_B R_B + A_{SW} R_{SW} + A_{BG} R_{BG} \tag{4}$$

where $\overline{R}_G$ is the modelled pixel reflectance for a given wavelength λ and $A_p + A_{s_s} + A_B + A_{SW} + A_{BG} = 1$ A represents area fractions of a pixel and R is reflectance. The subscripts P, S and B refer to several different trees (P: pine, S: spruce, B: birch), SW and BG refer to snow and bare ground respectively. For the mountainous areas the equation 4 is consist of snow and bare ground, since the trees are not available at high altitudes.

The visible band such as MODIS band 4 (0.555 μm) and a short-wave infrared band such as MODIS band 6 (1.640 μm) are retrieved from MODIS09GKM products. Rather than using MOD02HKM the atmospherically corrected MODIS09GKM data are used. The statistic-empirical correction method is applied for the visible channel. There is no exact relation between illumination and short-wave infrared band. Once the visible channel is corrected due to topographic effect, the reflectance values for snow and bare ground are retrieved from the satellite data considering the NDSI threshold greater than 0.4 for the horizontal slopes in the range of 0-5°. The final SCA represents the average fraction of snow covered ground for the calculation unit area.

4.3   Algorithms validation/heritage

Flat/forested areas

The method described above is based on a simplified reflectance model, which allows adaptation to local conditions (forest coverage) when estimating the fractional snow coverage. The limited number of reflectance contributors is essential in case of large application area and unknown target characteristics. Though not always 100 % accurate due to some necessary generalizations and basic assumptions, the method is statistically stable with 15-20 % average accuracy and, what is most important, applicable to areas with no auxiliary land cover or other information. The validation procedure is presented and tested in peer-reviewed paper: Metsämäki et al. 2005. Though focusing on AVHRR-data and 3rd order sub-drainage basins as unit areas, the article thoroughly covers the principle algorithm and the accuracy assessment, which both are perfectly suited for other optical data and for other unit areas as well. The MODIS-based algorithm is also presented in (Anttila et al. 2006), where the method is tested for Northern Manitoba area in Canada and the results were compared against NASA's snow maps. The method has been in operative use at SYKE from year 2002. Snow maps are provided on daily basis during the melting period each year. Since then, the major user has been the Finnish nationwide Hydrological simulation and forecasting system, which has gained clear advantage of the snow maps, resulting to improved forecasts (Metsämäki et al. 2005).

Mountainous regions

Fractional snow cover algorithm has been validated comparing the gained SCA-values against ground truth snow observations obtained from AWOS and individual snow measurements of the pilot area

(Karasu) in Turkey. ***Table 04*** shows the validation of the SCA values obtained for two dates (March 14 and March 30, 2006). The validation procedure will be applied for the whole year 2006.

Table 04 - The validation of the fractional SCA product with the ground observations

| AWOS		14 March 2006			30 March 2006		
Name	Elevation (m)	SD (cm)	SWE (mm)	SCA (%)	SD (cm)	SWE (mm)	SCA (%)
Hacımahmut	1965	14.5	58.0	73.9	-	-	-
Guzelyayla	2065	53.0	168.6	99.1	20.41	No obs	74.8
Ovacik	2130	67.7	209.2	100	64.8	245.2	94.9
Sakaltutan	2150	83.06	199.34	100	No obs	No obs	95.3
Cat	2340	93.75	335.8	100	91.89	349.2	95.9

5.   Merging products for flat/forested and mountainous areas

## 5.1   Merging according the H-SAF mountain mask

Although the products for flat/forested areas and for mountainous areas generated by FMI and TSMS cover the full H-SAF area, their quality differs in different areas, the product from FMI being tuned for flat/forested areas, that one from TSMS being tuned for mountainous areas. However, a single product is distributed to the users, obtained by merging the two products in such a way that in flat/forested areas the FMI product is captured, and in mountainous areas the TSMS product is captured. The distinction is determined by the "mountain mask" shown in Fig. 03, that was defined by METU.

The products from the institutes have different projections and nearest neighbourhood approach was selected for data co-location. The main idea of the merging algorithm is to minimize projection errors and try to reflect the strengths of the two algorithms in the final merged product. A mask based on digital elevation model (DEM) was used to separate the mountainous pixels from flat/forested areas. The merging algorithm finds the exact location of the non-mountainous pixels using this mask. These values are then replaced with the ones from the product for flat and forested areas.

The flow chart for calculating the look-up table is shown in *Fig. 12* and the merging procedure in *Fig. 13* (Ertürk 2009).
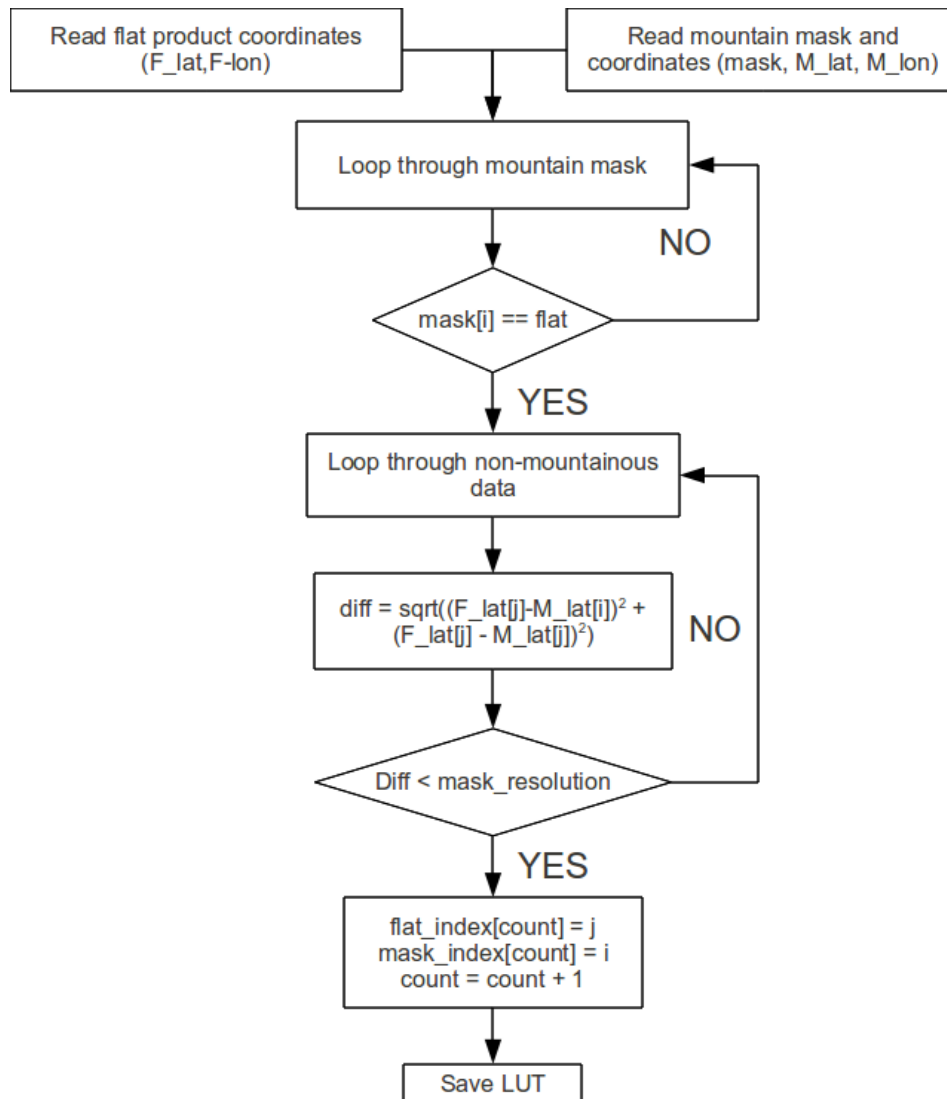
Fig. 12 - Generation of look-up table for merging mountainous and non-mountainous products.
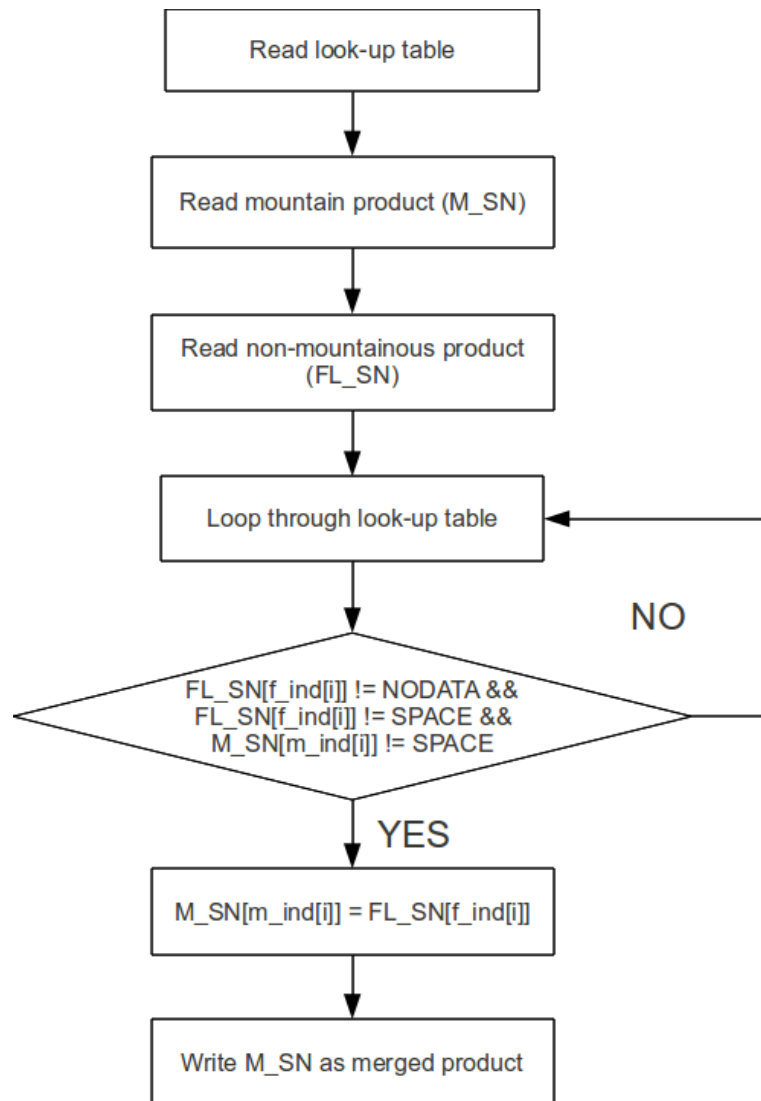
Fig. 13 - Flowchart of snow cover product merging.

## 5.2   Comparison with the GlobSnow mask   [METU]

[*Note - At the SVRR (System Validation Results Review) on 22-23 February 2010 the Board noted that a new mountain mask has been defined in the framework of GlobSnow, an ESA project coordinated by FMI and participated by NR (Norwegian Computing Centre), ENVEO IT GmbH, GAMMA Remote Sensing AG, Finnish Environment Institute (SYKE), Environment Canada (EC) and Northern Research Institute (Norut). The SVRR Board requested H-SAF to perform a comparison between the mountain mask adopted in H-SAF and that one defined by GlobSnow. The study was performed by METU and is reported here below*].

The HSAF and GlobSnow mountain masks have been compared and overlay analyses were made in order to depict the resemblances and differences of two mountain masks over the H-SAF domain (see *Fig. 14*).
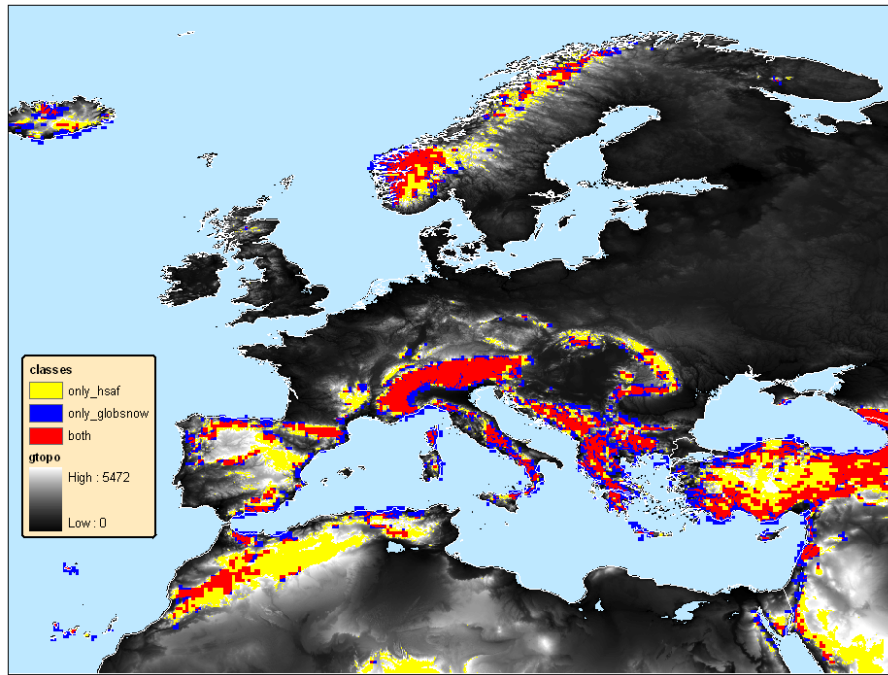
Fig. 14 - The overlay map of HSAF and GlobSnow mountain masks over GTOPO DEM.

At first glance, it could be observed that the common mountain area which is shown with red colour in the figure tells us that there is actually high aliasing between two masks, especially over higher elevations. The resolution of the GlobSnow mountain mask is 25 km since it was formed as EASE Grid format and due to its coarse resolution GlobSnow mountain mask defines mountains with less detail and shows significant amount of mountains over shorelines and sea as well. Some closer views and statistical analyze results are given in *Fig. 15*, *Fig. 16* and *Fig. 17*.
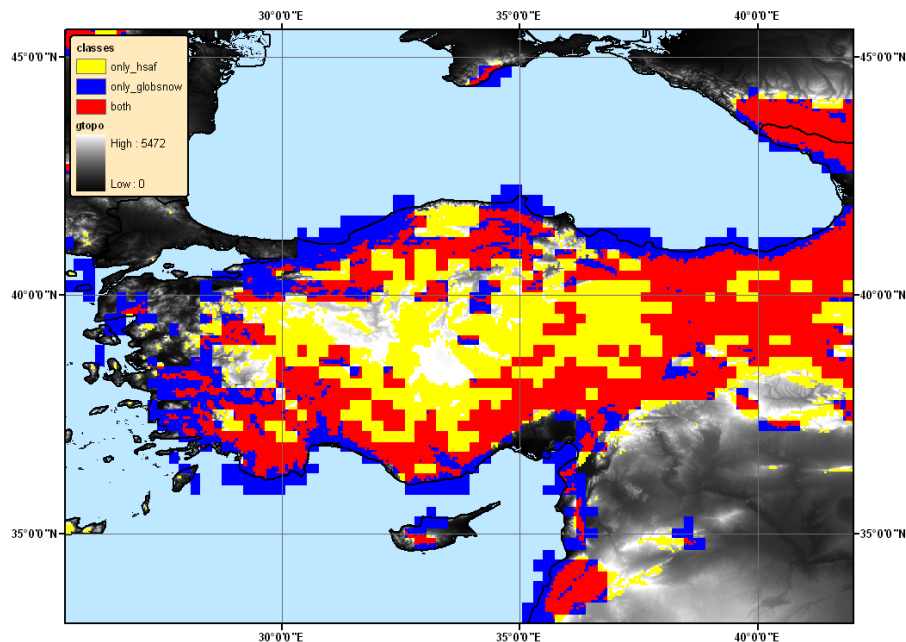
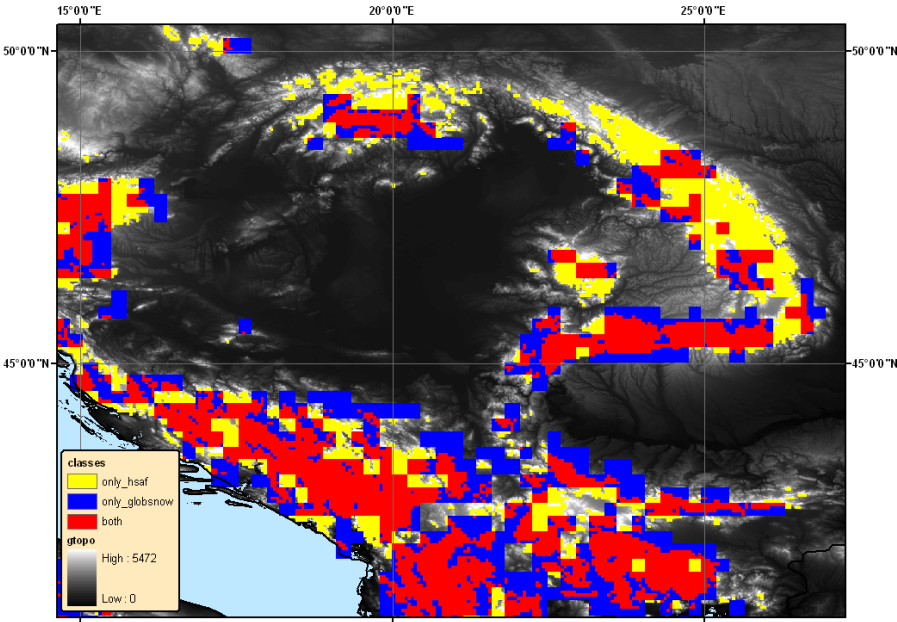**Fig. 15 - Closer view of overlay map focusing Turkey.**

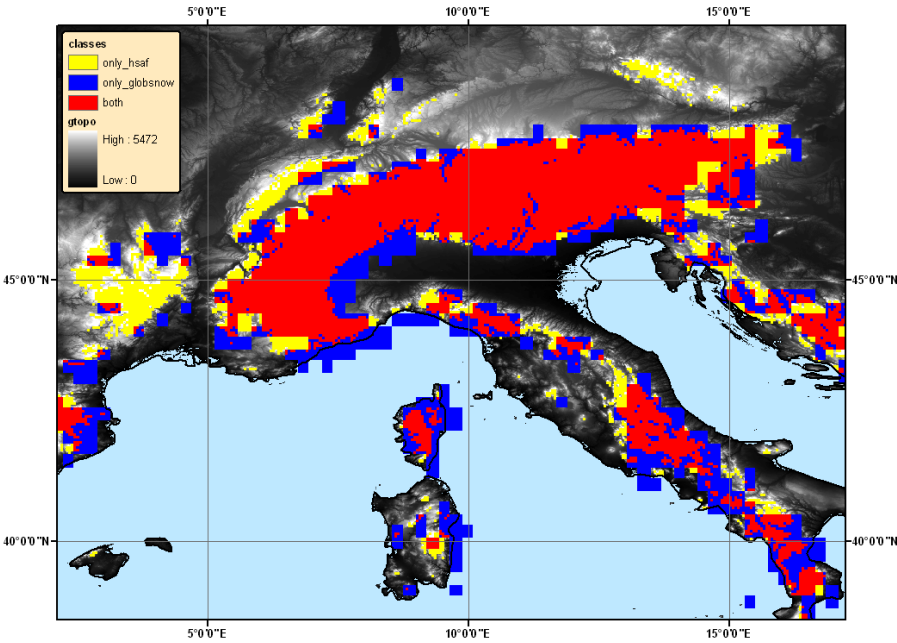**Fig. 16 - Closer view of overlay map focusing Tatra and Carpathian Mountains.**

Fig. 17 - Closer view of overlay map focusing Alps.

Statistical scores of the comparisons are reported in ***Table 05*** and ***Fig. 18***.

Table 05 - Statistical results of overlay analysis with GTOPO DEM over Alps

| VALUE	INHERIT	PERCENT	MEAN	STD	MEDIAN
1	Only H-SAF	13	919	280	898
2	Only GlobSnow	24	417	278	419
3	Both	63	1500	626	1420
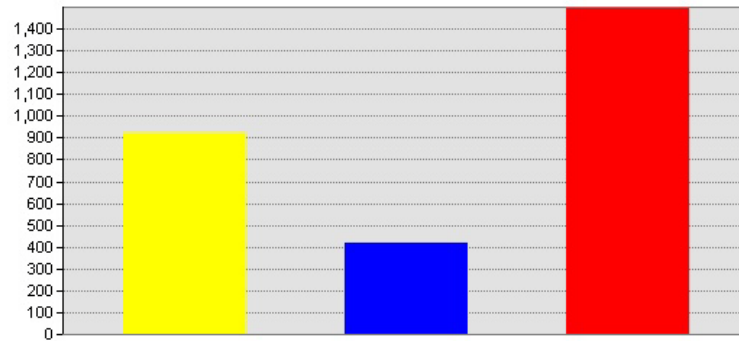
Fig. 18 - The mean values of 3 classes over Alps AOI.

An additional overlay analysis have been applied in order to have an idea about frequency of mountain mask pixels according to elevation zones covering all of the H-SAF domain. The results are given in tabular form in ***Table 06*** and as chart in ***Fig. 19***.

Table 06 - Percentages of mountain mask pixels over elevation zones

Elevation zones (m)	Only H-SAF (%)	Only GlobSnow (%)	Both (%)
0	0.03	21.48	0.08
0-500	1.84	42.68	3.22
500-1000	30.10	31.27	24.22
1000-1500	57.23	3.23	36.19
1500-2000	8.58	1.18	20.26
2000-2500	1.92	0.17	10.81
>2500	0.30	0.00	5.23
Total	100	100	100
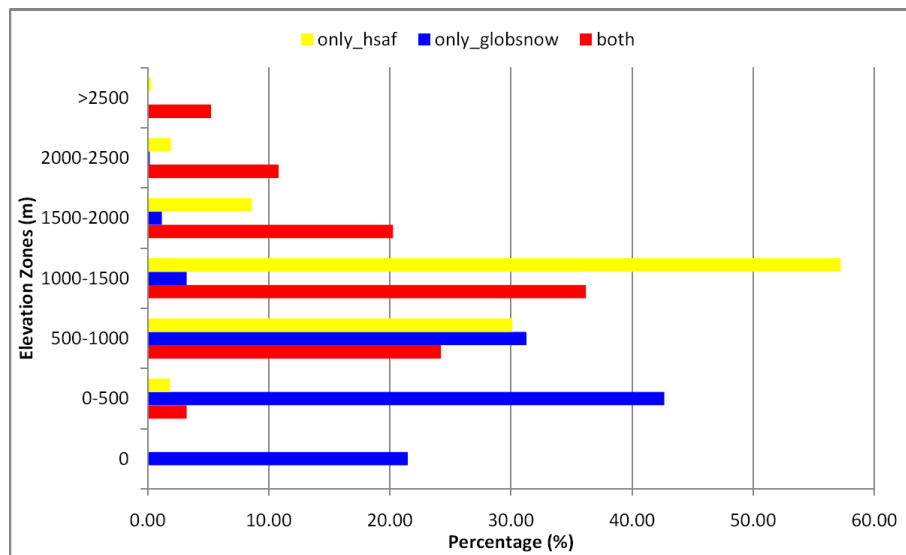
Fig. 19 - The areal distribution of masks over elevation zones.

As it can easily be observed from the figure that most of the pixels belonging to GlobSnow mountain mask are accumulated on lower elevation zones compared with H-SAF mountain mask. Moreover, there is no contribution of GlobSnow mountain mask over 2000 m due to missing high plateaus.

The figures given above analyzing two mountain masks with GTOPO DEM indicate the following additional facts.

Regarding to Fig. 15 which gives a closer view to Turkey, it is seen that the blue colours are mostly covering the areas close to shorelines even extending the land boundaries and overlaps with sea as well. In addition to this, the yellow colours are mostly high plateaus and they are missed by GlobSnow mountain mask which only uses "Slope > 2°" criteria while on the other hand the H-SAF mountain mask takes some additional parameters into account as it is given below:

"MEAN" $\geq$ 1000 m

OR

"STD_DEV" $\geq$ 2 % AND "MEAN" $\geq$ 700 m

OR

"RANGE" $\geq$ 800 m AND "MEAN" $\geq$ 500 m

Related with Fig. 16 that focuses on Tatra and Carpathian Mountains, it clearly shows that the hilly transitional areas are better covered with H-SAF mountain mask for Carpathian.

Finally and most importantly, when Fig. 17 is considered it is easy to observe a big similarity between two maps over main Alps region. On the other hand, some neighbouring mountain areas which are indicated with orange ovals are missed by the GlobSnow mountain mask. While statistical analysis results showed that common mountain areas that has 63 % (red colour) areal coverage with respect to all pixels, has 1500 m mean elevation as expected with a std of 626 m. With the help of additional criteria inclusion in its algorithm, H-SAF mountain mask covers additional 13 % of mountain area which has 919 m mean elevation and 280 m std. However, the blue pixels that are showing the mountain areas that only covered by GlobSnow mountain mask, are hard to be accepted as real mountain areas since they only have 417 m mean elevation and 218 std (also shown on Fig. 19).

The overall recommendation is to keep H-SAF mountain mask for snow products generation.
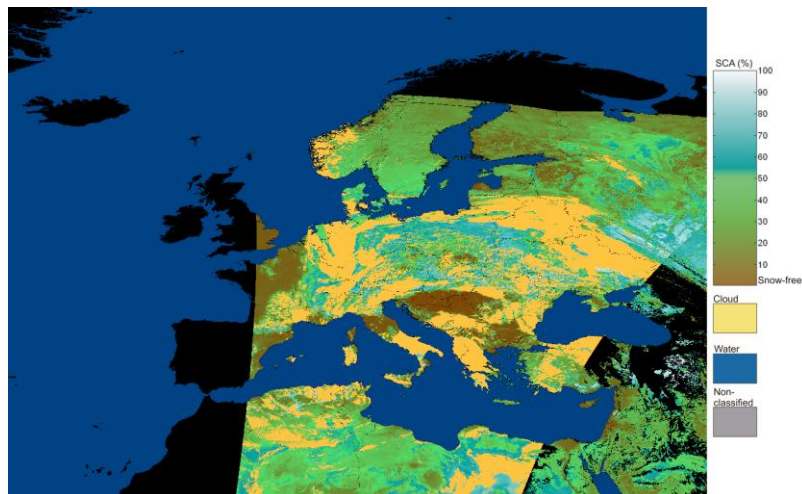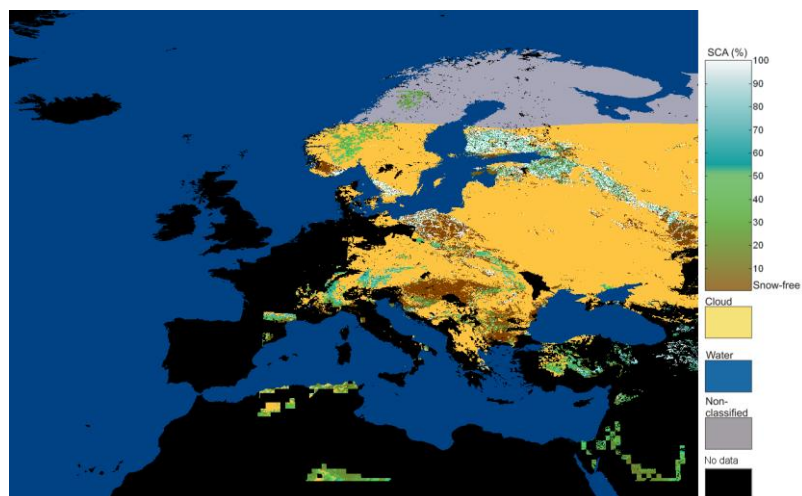
6.   Examples of snow cover maps

Fig. 20 shows examples of SN-OBS-3 products generated at FMI (flat and forested areas), at TSMS (mountainous area), and merged, for the same day. Maps are in *equal latitude/longitude grid*.
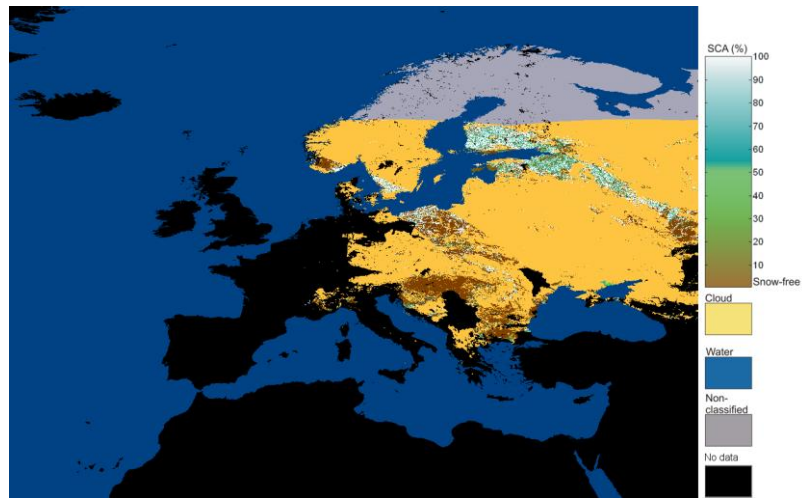
Processed product from FMI, optimised for flat and forested areas.

Processed product from TSMS, optimised for mountainous areas.

Merged product from FMI and TSMS.

Fig. 20 - Effective snow cover from NOAA and MetOp AVHRR - Time-composite maps over 24 hours, 6 March 2009.

References

Anttila S., S. Metsämäki and C. Derksen, 2006: "A Comparison of Finnish SCAmod Snow Maps and MODIS Snow Maps in Boreal Forests in Finland and in Manitoba, Canada". IEEE 2006 International Geoscience and Remote Sensing Symposium (IGARSS). Remote Sensing: A Natural Global Partnership. Denver, USA. 1-5.8.2006.

Hall D.K., R.E.J. Kelly, G.A. Riggs, A.T.C. Chang and J.L. Foster. 2002: "Assessment of the relative accuracy of hemispheric-scale snow-cover maps". *Annals of glaciology* 34:24-30.

Metsämäki S.J., S.T. Anttila, J.M. Huttunen and J.M. Vepsäläinen, 2005 "A feasible method for fractional snow cover mapping in boreal zone based on a reflectance model". *Remote Sensing of Environment*, **95**, 77-95.

Proy C., D. Tanre and P.Y. Deschamps, 1989: "Evaluation of topographic effects in remotely sensed data". *Reomete Sensing of Environment*, 30, 21-32.

Riano D., E. Chuvieco, J. Salas and I. Aguado, 2003: "Assessment of different topographic corrections in landsat-tm data for mapping vegetation types (2003)". *IEEE Trans. Geosci. Remote Sensing*, 41, 1056-1061.

Richter R., 1998: "Correction of satellite imagery over mountainous terrain". *Applied Optics*, 37, 18, 4004-4015.

Smith J.A., T.L. Lin, and K.J. Ranson, 1980: "The Lambertian assumption and Landsat data", *Photogrametric Engineering and Remote Sensing*, 46(9), 1183-1189.

Vikhamar D., R. Solberg and K. Seidel, 2004: "Reflectance Modeling of Snow-covered forests in hilly terrain" . *Photogrametric Engineering and Remote Sensing*, 70, 9, 1069-1079.

Warren S.G., 1982: "Optical properties of snow". *Reviews of Geophysics and Space Physics*, **20**(1), 2-52.